General Disclaimer

One or more of the Following Statements may affect this Document

- This document has been reproduced from the best copy furnished by the organizational source. It is being released in the interest of making available as much information as possible.

- This document may contain data, which exceeds the sheet parameters. It was furnished in this condition by the organizational source and is the best copy available.

- This document may contain tone-on-tone or color graphs, charts and/or pictures, which have been reproduced in black and white.

- This document is paginated as submitted by the original source.

- Portions of this document are not fully legible due to the historical nature of some of the material. However, it is the best reproduction available from the original submission.

Produced by the NASA Center for Aerospace Information (CASI)

OLD DOMINION UNIVERSITY RESEARCH FOUNDATION

Annual Report and Plans for

INTERDISCIPLINARY STUDY OF ATMOSPHERIC PROCESSES AND CONSTITUENTS OF THE MID-ATLANTIC COASTAL REGION

PERIOD COVERED BY REPORT: *June 1, 1974 - May 31, 1975*
PERIOD COVERED BY PLANS: *June 1, 1975 - May 31, 1976*

(NASA-CR-142820) INTERDISCIPLINARY STUDY OF ATMOSPHERIC PROCESSES AND CONSTITUENTS OF THE MID-ATLANTIC COASTAL REGION Annual Report, 1 Jun. 1974 - 31 May 1975 (Old Dominion Univ. Research Foundation) 43 p HC G3/44 N75-24120 Unclas 22892

Earl C. Kindle
Principal Investigator

Prepared for the
National Aeronautics and Space Administration
Office of University Affairs
Washington, DC

Under
Grant NGL 47-003-067

May 1975

Annual Report and Plans for

INTERDISCIPLINARY STUDY OF ATMOSPHERIC PROCESSES AND CONSTITUENTS OF THE MID-ATLANTIC COASTAL REGION

PERIOD COVERED BY REPORT: *June 1, 1974 - May 31, 1975*
PERIOD COVERED BY PLANS: *June 1, 1975 - May 31, 1976*

Prepared by the
Old Dominion University Interdisciplinary Team:

Faculty Participants

Dr. Earl C. Kindle - Physics & Geophysical Sciences
Dr. Alan Bandy - Chemistry
Dr. Gary Copeland - Physics & Geophysical Sciences
Dr. Roger Blais - Physics & Geophysical Sciences
Dr. Gerald Levy - Biology
Dr. Daniel Sonenshine - Biology
Dr. Donald Adams - Oceanography
Mr. George Maier - State Air Pollution Control Board

Prepared for the
National Aeronautics and Space Administration
Office of University Affairs
Washington, DC 20546

Under
Grant NGL 47-003-067

Submitted by the
Old Dominion University Research Foundation
P.O. Box 6173
Norfolk, Virginia 23508

May 1975

CONTENTS

Section		Page
I.	SUMMARY OF AY 1974-75 EFFORT	1
II.	PLANS FOR THE FORTHCOMING YEAR	3
III.	BUDGET	5

Attachments

1. MAPPING FOREST VEGETATION WITH ERTS-1 MSS DATA AND AUTOMATIC DATA PROCESSING TECHNIQUES

2. USE OF LARS SYSTEM FOR THE QUANTITATIVE DETERMINATION OF SMOKE PLUME LATERAL DIFFUSION COEFFICIENTS FROM ERTS IMAGES OF VIRGINIA

3. DATA SET FOR CRANEY ISLAND OIL REFINERY INSTALLATION EXPERIMENT (separate volume)

4. DATA SET FOR BACKGROUND INVESTIGATION OF ATMOSPHERIC CONSTITUENTS FOR NANSEMOND RIVER SITE (separate volume)

5. DATA SET FOR BACKGROUND INVESTIGATION OF ATMOSPHERIC CONSTITUENTS FOR RICHMOND, VIRGINIA AREA (separate volume)

I. Summary of AY 1974-75 Effort

1. Field Experiments - Four major field experiments were conducted in response to specific requests from the State Air Pollution Control Board. These included

a. Nansemond River Experiment - June 8 to July 22, 1974; to derive background data for installation of new proposed oil refinery.

b. Fort Story Experiment - July 20 to August 10, 1974; to provide background data for proposed Navy Housing Project.

c. Richmond Experiment - September 25 to October 21, 1974; to derive background data for photo-chemical oxident problem in the Richmond area.

d. Craney Island Experiment - Follow on background data for proposed oil refinery.

The data sets for these experiments were all required to meet rigid time deadlines and were submitted to the Virginia State Air Pollution Control Board according to schedule. Copies of these data sets are attached.

2. Biosphere component - For further investigations into the natural hydrocarbon emissions in the area, an extensive program for characterizing the emission species of the Great Dismal Swamp was conducted. The primary base for this investigation was the LARS output for the ERTS system, and field data collected by team personnel. Results from this experiment were published in the Proceeding of the Remote Sensing Conference and a copy is attached to this report.

3. Remote Sensor Analysis of Smoke Plumes - Several additional studies of smoke plumes were conducted and a paper was presented

and published in the Proceedings of the Remote Sensing Conference and is attached to this report.

4. Other products of the Program. In addition to the direct support of the State Air Pollution Control Board, the following additional results have been realized:

a. Five M.S. Degree Theses have been prepared through the efforts of this program.

b. Four papers have been published in proceedings at National Meetings.

c. Six presentations have been made at national meetings and five at Virginia Academy of Science or local meetings.

d. ODU has developed a sizeable Remote Sensing Laboratory and has introduced two courses on Remote Sensing Technology to serve the entire University. These courses experienced enrollment of 45 students at their first offering.

e. An aerial and satellite photograph data base for the Hampton Roads area has been collected and will result in the publication of seven additional papers and two more M.S. theses which are underway at this time.

f. Personnel in the program have completed (to our knowledge) the first successful application of ERTS data to air pollution. (See attached publication).

g. A new multidisciplinary M.S. degree program will be introduced at the University directed toward environmental analysis. The three core sub-disciplines of this program are:

1) Atmospheric Science

2) Land Use

3) Remote Sensing Technology

II. Plans for the Forthcoming Year.

1. Field Experiments

a. To fulfill our commitment to the State Air Pollution Control Board, one major field experiment will be conducted in June 1975. This experiment is in response to a specific request by the Director of District VI of the State Air Pollution Control Board and will be concerned with the pollutants from "Money Point", a major pollution service for the Hampton Roads area.

b. Additional field experiments are being planned but because of reduced funding and the need to apply a heavier amount of project efforts to data set analysis, these will require some expendable supply support from the SAPCB.

2. Natural Emission Sources - The biosphere component will be concerned with the completion of the Great Dismal Swamp analysis program and integration of results with ERTS classification of emitters with the mobile laboratory data.

3. The meteorological support component will concentrate on the adaption of our numerical model to the Money Point experiment and the integration of the LARS output of ERTS data into this experiment.

4. The remote sensor analysis of smoke plumes phase will work with the major field experiment data for June but for most of the year will be concerned with a further application of LARS/ERTS data. By our project's participation in the LARS program, we have obtained a sizeable data set of digitized ERTS data which includes several plume and smoke pollution cases.

5. General Follow-on Program concept - Compared to previous years, we shall devote an increased effort to the analysis and diagnosis of the extensive data sets we have collected to date.

The heavy priority for background data imposed by the State Air Pollution Control Board has made it necessary to focus our attention to field experiments and postpone the thorough scientific analyses of the data. Accordingly, for this and the final year of the program, we shall proportionately decrease our data collection efforts and increase our analysis and publication efforts.

III. Budget

A. Budget for Individual Components

1) Component A — Drs. Copeland and Bandy

Dr. Gary Copeland Summer 1975 (50% time)	$ 2317
Dr. Alan Bandy Summer 1975 (50% time)	2483
Graduate Student Summer 1975	1250
Undergraduate Student (2) Summer 1975	1600
Total Salaries	$ 7650
Indirect Costs	3045
Travel	500
Supplies	2000
Equipment	1800
TOTAL	$14,995

2) Component B — Drs. Blais and Copeland

Dr. Roger Blais Summer 1975 (50% time) AY 1975/76 (25% time, 8% NASA, 17% ODU)	$ 2083 1112
Dr. Gary Copeland AY 1975/76 (25% time, 8% NASA, 17% ODU)	1188
Undergraduate Student AY 1975/76 Summer 1975	580 400
Indirect Costs	2124
Supplies	200
TOTAL	$ 7687

3) Component C Dr. Earl Kindle

Dr. Kindle	
Summer 1975 (50% time) AY 1975/76 5% time ($1535 ODU contribution)	$ 4700
Undergraduate student	
Summer 1975	640
AY 1975/76	600
Total Personnel	$ 5940
Equipment (CO Monitor)	5500
Supplies	527
TOTAL	$13,792

4) Component D Drs. Levy and Sonenshine

Personnel	$ 2500
Supplies	1410
Equipment	300
Publications	1300
Indirect Costs	990
TOTAL	$ 6500

5) Component F Dr. Kindle	
Data Handling	$ 1200
Secretary	500
5% Dr. Kindle AY time ($1535)	
Total Personnel	1700
Indirect Costs	673
Travel	700
Consulting and Programming Services	831
Equipment Maintenance	1500
Publications	1000
Supplies	110
TOTAL	$ 7014

D. Composite Budget

Salaries	$ 23,153
Travel	1,200
Supplies & Maintenance	5,747
Equipment	7,600
Publications	2,300
Consultant Service	831
Indirect Costs	9,169
TOTAL NASA Contributions	$ 50,000

ODU Contributions (Drs. Kindle, Copeland and Blais partial salaries and indirect costs $8,967.00)

TOTAL BUDGET	$ 58,967.00

Attachment 1

MAPPING FOREST VEGETATION WITH ERTS-1 MSS DATA AND AUTOMATIC DATA PROCESSING TECHNIQUES

MAPPING FOREST VEGETATION WITH ERTS-1 MSS DATA AND AUTOMATIC DATA PROCESSING TECHNIQUES

J. Messmore*, G. E. Copeland† and G. F. Levy∆

Department of Biology
and Department of Physics and Geophysical Sciences
Old Dominion University, Norfolk, Virginia

Abstract

This study was undertaken with the intent of elucidating the forest mapping capabilities of ERTS-1 MSS data when analyzed with the aid of LARS' automatic data processing techniques. The site for this investigation was the Great Dismal Swamp, a 210,000 acre wilderness area located on the Middle Atlantic coastal plain. Due to inadequate ground truth information on the distribution of vegetation within the swamp, an unsupervised classification scheme was utilized. Initially pictureprints, resembling low resolution photographs, were generated in each of the four ERTS-1 channels. Data found within rectangular training fields was then clustered into 13 spectral groups and defined statistically. Using a maximum likelihood classification scheme, the unknown data points were subsequently classified into one of the designated training classes. Training field data was classified with a high degree of accuracy (greater than 95%), and progress is being made towards identifying the mapped spectral classes.

---

* Graduate Student, Department of Biology
† Assistant Professor, Department of Physics and Geophysical Sciences
∆ Associate Professor, Department of Biology

J. Messmore, G. E. Copeland and G. F. Levy

Introduction

A great impetus to the field of remote sensing was realized in July of 1972 with the launch of the Earth Resources Technology Satellite (ERTS-1; now designated LANDSAT-1). Since that date, large quantities of digital imagery have been generated, though the applicability of this satellite data to specific problems remains to be fully investigated.

Computer-aided analysis of ERTS-1 data, as applied to forest mapping, has not been extensively investigated and comparatively little has been published on this phase of satellite data application. However, Erb (1973) utilized ERTS-1 data to detect, identify, and measure forest and agricultural features of interest. In addition, Heath and Parker (1973) used automatic computer processing techniques to map timber stands and range plants in the Houston, Texas area.

This study examines the feasibility of applying ERTS-1 MSS data and automatic data processing techniques as a means of mapping forest vegetation. The site for this investigation is the Great Dismal Swamp, a 210,000 acre forested area which transects the Virginia-North Carolina border. This region is of special interest, as it is one of the last large wilderness areas remaining along the Middle Atlantic coastal plain (Fig. 1). Due to its unique geographic location, both northern and southern flora can be found growing there. Meanly (1973) characterized the Great Dismal Swamp's vegetation as having five major plant communities: 1) Hydric or deep water swamp, 2) Semihydric or mixed swamp forest, 3) Mesic forest, 4) Atlantic white cedar forest, 5) Evergreen shrub bog or pocosin. To date, application of ERTS-1 data to specific studies within the swamp is limited to the hydrologic and vegetational investigations of Carter in 1974.

Being the wilderness it is, the Great Dismal Swamp lends itself well to remote sensing studies. Many interior regions are largely inaccessible to ground survey and, consequently, little is known about these areas. Through the use of remotely sensed data, such as ERTS-1, the need for large amounts of expensive and time consuming ground-obtained data can be minimized.

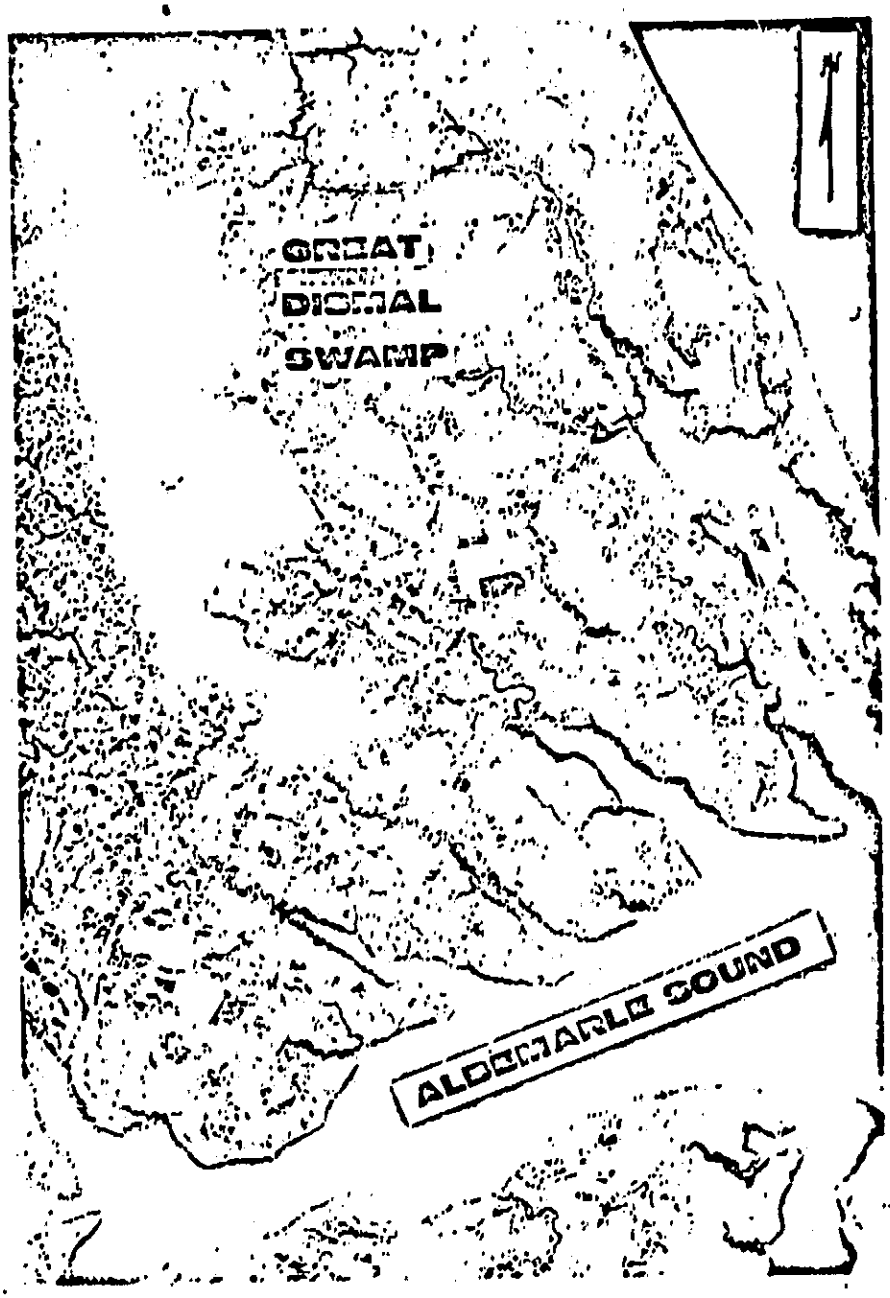

Fig. 1 A portion of ERTS image No. 1205-15150 (MSS 5) acquired on Feb. 13, 1973. (In the current study, August data was utilized.)

ORIGINAL PAGE IS
OF POOR QUALITY

Materials and Methods

On August 30, 1973, ERTS-1 remotely acquired data of an area 100 x 100 nautical miles on the eastern coast of the United States. Contained within this MSS data was the study site of this investigation, the Great Dismal Swamp (See Figure 1). Analysis of the spectral data obtained over the swamp was accomplished through the use of automatic data processing techniques developed by the Laboratory for Applications of Remote Sensing at Purdue University. Access to these ADP techniques was provided by a remote computer terminal located at the NASA Langley Research Center, Hampton, Virginia.

Generally, an unsupervised classification scheme, such as applied in this research, begins by defining as training fields those areas within the study site that contain representative vegetative cover. This information is then divided into "X" number of clusters based on the distribution of spectral information within the training field data. The reflectivity of each cluster or spectral class is then defined in terms of its mean vector and covariance matrix. The data points representing unknown ground features within the area to be mapped are subsequently classified into one of the user-defined spectral classes by a pattern recognition algorithm. Final analysis centers upon determination of the relationship between the mapped spectral classes and known surface data, i.e., ground truth comparison.

Pictureprint. The first computer program to be run in this study was the picture-print function. This program produces a gray scale printout of the digital data from one channel of the ERTS multispectral scanner. Various shades of gray are represented by specific alphanumeric symbols. These are assigned so that highly reflective areas are represented by a symbol which covers a low percentage of the printout, such as . . . ; absorbent terrain is differentiated from other areas by assigning a dense appearing symbol, e.g., BBBB. Because spectral information representing ground terrain will not be evenly distributed between the highest and lowest reflectance values, the data is histogrammed. Symbols are then assigned to radiance values such that each has approximately the same probability of being printed. As an interpretive tool, the pictureprint can be very useful in developing a grasp of the data's spatial orientation and in locating areas of known composition.

Cluster. After designating training areas to the

computer, the cluster function is run. This program is necessary because the pattern recognition algorithm assumes that each spectral class can be characterized by a multidimensional Gaussian density function. The dimensionality of this space is the number of distinct spectral bands present in the imagery (ERTS-1 has 4 bands). Clustering the training data gives an indication of whether or not the data tends to be Gaussian and provides a means for dividing it into approximate Gaussian sub-classes if the original data is non-Gaussian (Lindenlaub, 1973). Options available within the cluster function allow the researcher to choose any combination of available spectral bands, as well as the number of cluster groups to be separated within the data. The cluster function output, in addition to providing maps of the clustered data, also provides a listing of the pairwise separability values. This information is useful in determining the uniqueness of spectral clusters within the training field data.

Statistics. This processing function provides an estimate of each training classes' mean vector and covariance matrix. These statistics are usually supplied in the form of punched output cards which are used in later analysis steps. Additionally, the statistics function will produce training class histograms in user-designated channels. These histograms serve as a partial check as to whether each training classes' data is Gaussian (unimodal) in nature. Serious departure from a Gaussian distribution may necessitate refinement of the training class data.

Feature selection. The feature selection program assists the analyst in finding the middle ground between greater classification accuracy and increased computer time. The program calculates the statistical distance in N-dimensional space (N=# of channels) between the training classes provided. The requested channel combinations are then ranked in terms of the average or the minimum pairwise distance between all pairs of classes. If the statistical distance between significant spectral class pairs is low, it may be necessary to repeat some of the previous analysis steps.

Classification. Classification of the unknown data is the last step in the analysis sequence and represents the culmination of all previous analyses. Program inputs include the statistics deck, the selected combination of channels, and coordinates of the area to be classified. The pattern recognition algorithm, as applied in this study, individually classifies each pixel into one of the statistically defined training classes on a maximum likelihood basis. The output of

the classification function, combined with a printresults program, results in a classification map with alphanumeric symbols representing the designated spectral classes.

An option that must be considered prior to actual generation of classification maps is thresholding. If this option is not applied, the classification algorithm will classify every data point into the class it most nearly resembles, even though the resemblance may be quite remote. Thresholding allows the researcher to arbitrarily screen out those picture elements not demonstrating a high degree of correlation with user-designated spectral classes. Thresholded points then appear as blank spaces on the final classification map.

Results and Discussion

August 30, 1973

The initial analysis step obtained gray scale printouts of the study area in all four ERTS-1 channels. These printouts were then compared with black and white, color and color IR aerial imagery of the swamp. Pictureprints of the data in channels 1 and 2, 0.5 - 0.6 μm and 0.6 - 0.7 μm respectively, produced the best delineation of swamp boundaries with the Suffolk scarp on the swamp's western edge being clearly defined. In addition, U.S. route 460 and the Norfolk and Western railway were discernable cutting east to west across the northern region of the swamp. Pictureprints produced of channels 3 and 4, 0-7 - 0.8 μm and 0.8 - 1.1 μm respectively, were especially useful in the delineation of water, due to its high absorbancy in these wavelengths. Lake Drummond, located in the swamp's center was clearly differentiated from the surrounding forest, however, none of the numerous drainage ditches located in the swamp could be identified. This is believed to be due to tree overhang and the characteristic low water levels of the swamp in August.

In order to determine the distribution of spectral information taken over the swamp, the clustering algorithm was run on eleven training fields (15,894 data points). Cluster results maps were then printed which contained alphanumeric symbols indicating the geographic location of spectrally similar materials. Clustering performed with all four wavelength channels was not found to be optimal for obtaining spectral separability within the forested training area. Comparison of the cluster means and standard deviation values in all four channels revealed the reason for this less than optimal

cluster separability. Within channels 1 and 2 the cluster radiance means were nearly identical, thereby causing a large amount of data overlap in two of the four clustering space dimensions.

Through elimination of channels 1 and 2 in the clustering process, the number of separable clusters was increased. This is illustrated by comparing the separability quotient values for a four channel cluster run versus a two IR channel cluster run. A value of 0.75 is often used as the breakthrough point for cluster separability. Upon examination of a "maxclas (12)" cluster run, it was determined that fifteen of the separability quotient values were less than 0.75. However, one value of less than 0.75 resulted from two IR channel clustering.

Further analysis of the two IR channel clustering suggested the presence of approximately thirteen spectral groups which were provided to the statistics processor. In addition to calculating the mean vector and covariance matrix for each of the thirteen forest classes, the statistics processor was requested to graph histograms of each training class in all four channels. These histograms were printed so that the distribution of spectral data within each class could be examined. It was found that each class was distributed in an approximate Gaussian manner in all four channels. The statistics processor also produced a coincident spectral plot, which illustrated the relative amplitude of each classes' spectral response in each of the four ERTS-1 channels. Generally, channels 1 and 2 were incapable of differentiating one forest class from another. This was because the class radiance value distributions overlapped one another in these two channels. Channels 3 and 4, on the other hand, contained a wider range of mean spectral values and, therefore, demonstrated the ability to distinguish between the thirteen forest spectral classes.

The next step of the analysis, feature selection, was used to determine the combination of available channels that would yield the most accurate classification results with a minimum amount of computer time. The statistical figure of merit calculated by this function is transformed divergence (Swain 1973). It is a "measure of the dissimilarity of two distributions" and "provides an indirect measure of the ability of the classifer to discriminate successfully between them". The strategy utilized was to weight all classes equally and maximize the pairwise transformed divergences.

Table I gives a summary of three computer experiments.

TABLE I

ERTS CHANNELS USED	TRANSFORMED DIVERGENCE AVERAGE	MINIMUM
1, 2, 3, 4	1960	1204
3, 4	1954	1169
1, 2	432	18

Even though the final classification used all four ERTS bands, clearly the IR bands alone would produce essentially the same classification. Once again, the redundant information content of channels 1 and 2 clearly indicate failure for spectral classification schemes based wholly on these bands for this application.

In the last step of the analysis sequence, the classification algorithm, in conjunction with the printresults function, generated a map-like display. Each spectral class was depicted by a user-defined alphanumeric symbol. These symbols were changed throughout the study in an attempt to bring about easier visual pattern detection. Overall training field classification performance was 96.0%; a figure that indicates the pattern recognition algorithm encountered very little confusion in the mapping of training field data. Application of an arbitrary threshold value (2.0) easily differentiated materials dissimilar to the mapped forest classes. Lake Drummond, located in the swamp's interior, was correctly thresholded, as well as US route 460 and agricultural fields which delimit the swamp on the east, west and south.

Subsequent analysis of the classification map necessarily centered upon determination of the correspondence between spectrally similar ground cover (the map symbols) and categories of informational value, e.g., deciduous or coniferous forest, stand density, etc. Spectral class thirteen, exhibiting the most absorbent qualities of the mapped spectral classes, corresponded closely with dense, monospecific stands of Atlantic white cedar (Chamaecyparis thyoides). Misclassifications did occur, however, and these were observed primarily in two different areas. Several solitary incorrect mappings were noted around the shores of Lake Drummond, a phenomena which can be attributed to pixel

averaging the reflectance of water and forested terrain. Misclassifications also occurred within agricultural fields adjacent to the swamp. These incorrect mappings may be due to the presence of standing water in the fields at the time of satellite data acquisition. Spectral class twelve most closely corresponded to forest stands dominated by Atlantic white cedar, but interspersed with a mixture of hardwoods (mostly Red maple, Acer rubrum, and Sweet gum, Liquidambar styraciflua). By mapping the combination of spectral classes twelve and thirteen, a good representation of Atlantic white cedar present in the swamp has been attained. (See Figure 2).

Further research concerning correspondence between the remaining eleven spectral classes and actual forest cover is progressing, though some problems have been encountered. Unlike the Atlantic white cedar stands which occur as monospecific communities, other plant communities within the swamp are characterized by the presence of several tree and/or shrub species. This leads to a situation of complexity and natural randomness that makes classification into meaningful categories difficult. Problems have also been encountered in attempting to locate, with any degree of certainty, the position of specific forested areas in the ERTS digital data. This is primarily due to: (1) the northeast-southwest skew contained in ERTS-1 MSS data; (2) a lack of large, identifiable land features within the swamp (except Lake Drummond); (3) rectangular computer output format. These problems have been solved to a degree, in that locations in the ground scene can now be generated by an affine mapping transformation developed by Blais (1975).

Another difficulty inherent in mapping diverse vegetation with low resolution scanner data includes pixel averaging. Because tree and shrub species that comprise the swamp's plant communities are much smaller than the 80 meter square pixel size, and are unevenly distributed, spectral characteristics recorded by the scanner will not always be an accurate indicator of a specific species composition. Hypothetically, at certain times of the year, a pixel containing a mixture of 25% Loblolly pine (Pinus taeda), and 75% Red maple may have average reflectance characteristics identical to a pixel averaging the reflectances of 50% Yellow poplar (Liriodendron tulipifera), and 50% Sweet gum. Of course, temporal scanner data obtained during subsequent seasons of the year may remove this spectral signature ambiguity. Heller (1973), using photogrammetric techniques, reported

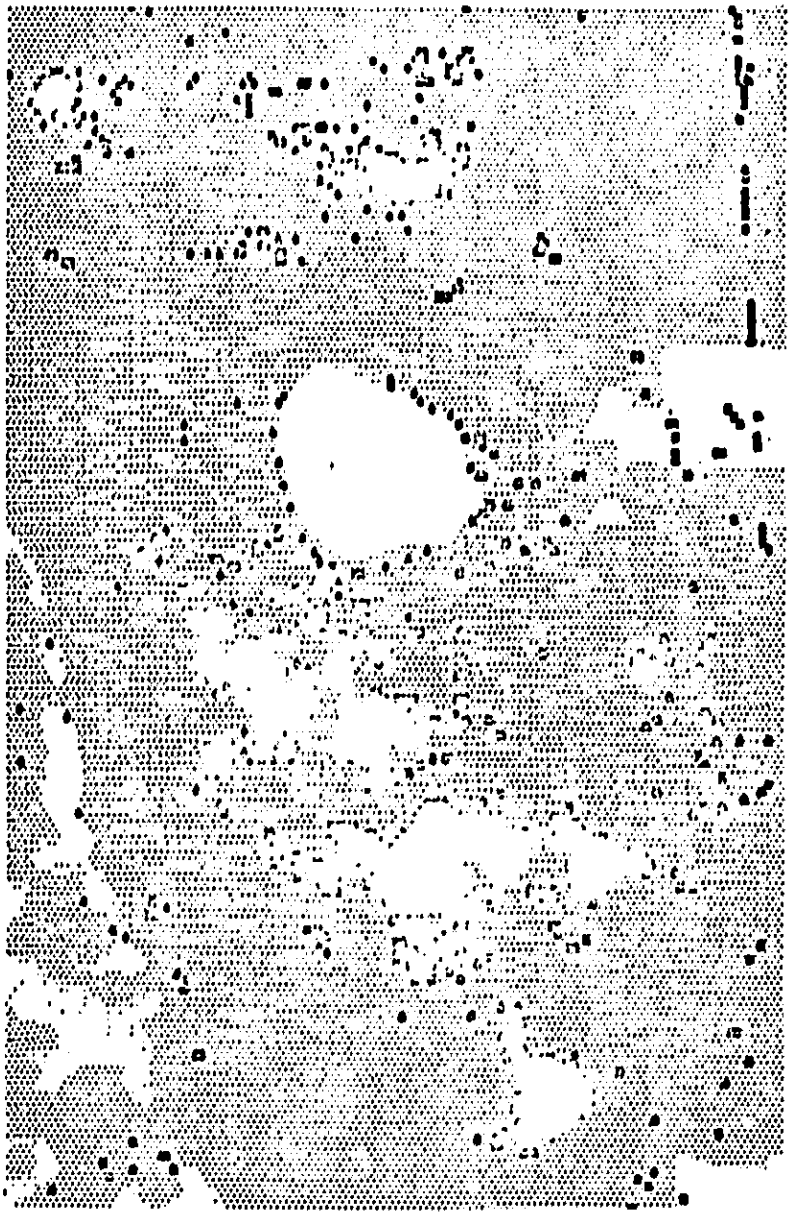

Fig. 2 Classification map of the Great Dismal Swamp (dark regions indicate Atlantic white cedar, thresholed pixels occur as blank areas). Lake Drummond is the central oval feature. North is towards the top.

ORIGINAL PAGE IS
OF POOR QUALITY

that forest discrimination with ERTS-1 data was poorest during the summer months (the season during which this study's data was taken) and yielded the best results during spring, fall, and winter). This lends support to the idea that accurate classification of the swamp's vegetational communities will require analysis of data acquired during two or more seasons of the year.

Seasonal Analysis (Aug. 30, 1973 and Oct. 10, 1972)

Even though ERTS is in a sun-synchronous orbit, illumination of the ground scene does change seasonally due to motion of the sun on the ecliptic and variations in the sun-earth distance. Moreover, the spectral reflectivities of different ground features change with many variables, i.e., temperature, moisture content, time in growing season, meterological visibility, etc. Additionally, since the solar elevation angle changes, the scattering angle changes. All of these factors contribute to changes in scene-to-scene radiance values of any one ground feature.

As a first attempt at modeling this complex phenomena, it was deemed desirable to calculate the undepleted insolation at image time. Using the method described by Smart (1965) a computer program was written to provide the undepleted insolation (top of atmosphere) for any location on the earth as a function of time in a year at image time for the ERTS passes. Additionally, the total daily insolation curve for each location is provided. Figure three gives these results for the Dismal Swamp at 1515 GMT as a function of days past perihelian passage (Jan. 4, 1973). The Aug. 30, 1973 date is noted.

Since ERTS MSS sensors have sensibly square response functions over their active spectral range, the signals obtained by each band for a white viewing scene is then just the integral of the solar black body over the response function. Assuming a 5750K solar black body, this integration of the Planck function leads to the values listed in Table II for the energy flux in each sensor.

Table II

Band Wavelength Microns	% of a 5750°K Black Body	Maximum Radiance MW/cm^2-SR
.5 - .6	12.9	2.48
.6 - .7	11.4	2.00
.7 - .8	9.5	1.76
.8 - 1.1	18.5	4.60

The field of view is constant for all sensors, and thus the signal outputs for a viewing surface whose albedo is one (total reflection) will fall into those ratios.

In an attempt to determine seasonal fluctuations of LARS statistics, two ERTS images were examined (August 30, 1973 frame number 1403-15132 and October 10, 1972 frame number 1079-1514). Identical training fields were used and the radiance means and standard deviations were generated for six forest spectral classes for those two dates. Table III gives the means for each date, band, and class, as well as the average over classes of the standard deviations for each band.

Table III
Forest Spectral Class Statistics

	Aug 20, 1973				Oct 10, 1972			
	Band							
Class	1	2	3	4	1	2	3	4
1	26.61	15.91	43.43	25.78	19.83	10.91	35.04	22.48
2	26.14	15.44	42.33	24.09	18.98	10.98	33.32	20.72
3	26.06	15.17	41.06	24.14	19.69	10.71	31.54	21.37
4	26.13	15.61	38.94	22.50	19.87	11.06	30.50	19.41
5	26.46	15.60	40.18	23.00	19.42	10.88	28.88	18.26
6	26.47	16.91	37.62	21.12	19.21	10.82	26.29	16.94
<σ>	0.23	0.61	2.15	1.58	0.36	0.12	3.13	2.06

Seasonal differences are traceable to many variables. A major difference for scenes imaged on different dates is the solar illumination. The ratio of the undepleted insolation at image times for the two dates was determined to be (i = August 30, 1973; j = October 10, 1972).

$$\frac{Ii}{Ij} = 1.244 \qquad \text{(eq. 1)}$$

This is also the ratio of the cosines of the solar elevation angles at image time. Calculation of percent differences of

the forest class means at the two dates to the insolation ratio, yields a first estimate of class changes between image time. Table IV lists this ratio

$$(((\mu_i/\mu_j) - 1.244)/1.244) \times 100 \qquad \text{(eq. 2)}$$

for each class and band. If this percentage is positive, the August 30 image is brighter than the insolation corrected October 10 image.

Table IV
Per Cent Difference

Class	Band 1	2	3	4
1	+7.8	+17.2	-0.4	-7.8
2	10.7	13.0	+2.1	-6.54
3	6.4	13.9	4.6	-9.2
4	5.71	13.4	2.6	-6.8
5	9.5	15.3	11.8	+1.3
6	10.7	25.6	15.0	+0.65

In order to estimate the magnitude of seasonal differences, a knowledge of some environmental parameters is required (see Table V). Meteorological data is from Norfolk Regional Airport located about 25 km NE of the training fields. The optical depth, τ, is calculated from the work of Potter and Shelton (1974) for the known visibility. The precipitable water layer is deduced from radiosonde and the TSTSP (Total sun target satellite path water amount) is determined in the method of Pitts, McAllum and Dillinger (1974).

Table V
Environmental Parameters

	Oct. 10, 1972	Aug. 30, 1973
Optical Depth (0.5 μ)	0.30	.49
Dew Point (°C)	5	25
Temperature (°C)	13.9	31.1
Absolute Humidity (gm/m^3)	6.6	22.6
Visibility (km)	24.1	1.6Fog
Percipitable water layer (cm)	2.0	5.8
Coefficient of Haze (cohs)	0.6	
Wind azimuth (°)	10	10
Speed (knts)	15	4
Solar Elevation	40°	52°
TSTSP (cm)	5.11	13.2

J. Messmore, G. E. Copeland, and G. F. Levy

Effects of Haze

Potter and Shelton have done a study on the effects of atmospheric haze and varying sun angles on the LARS classification accuracy for corn and soybeans. Since both Raleigh and Mie scattering are inversely proportional to the fourth power of wavelengths, it is to be expected that for fixed solar angles, the scattering activity of atmospheric haze will increase the radiance of ERTS scenes most in MSS band 4 and least in MSS 7. Examination of their results for optical depth with meteorological visibility, yields a value of $\tau = 0.3$ for October 10, 1972. Calculation of τ for August 30, 1973 from visibility is not useful, since a fog bank was adjacent to the airport.

Potter and Shelton give tabular results for the variation of class means μ, with optical depth, τ, for corn and soybeans for each ERTS band. Fitting their results in a least squares linear regression yields

$$\mu \text{ (corn)} = 17.86\ \tau + 22.18$$

$$\mu \text{ (soybeans)} = 17.35\ \tau + 23.30 . \qquad \text{(Eq. 3)}$$

over the range $\tau = 0$ to 0.4. If we assume that the average of the slopes (17.51) is appropriate for our forest classes, and using $\tau = 0.3$ for the October 10 optical depth, then the haze free values of the October 10 class means is given by (MSS 4)

$$\mu_j \text{ (haze free)} = \mu_j - 5.25 \text{ (eq. 4)}$$

Correcting for insolation differences, we deduce the August optical depth (MSS 4) to be

$$\tau_i = \frac{\mu_i - 1.244\ \mu_j \text{ (haze free)}}{17.51} \qquad \text{(Eq. 5)}$$

This assumes that the reflectance is constant in time for a given spectral class. Calculations for each class, however, yield almost identical values of τ_i (0.49 ± 0.03). Using an empirical relationship between coefficient of haze (cohs), mass loading, and visibility, indicates τ for this date as 0.5. Similar results are possible for other ERTS bands but the effect is progressively smaller with increasing band number.

Examination of Table IV (MSS 4) for all six forest classes, thus indicates the increased radiance can nearly all be accounted for by an increased optical depth, i.e., aerosol loading. This is quite realistic since: the air is of maritime origin; the relative humidity is high (77%); air temperature is 88°F; and contrast in the MSS 4 imagery is reduced over October imagery.

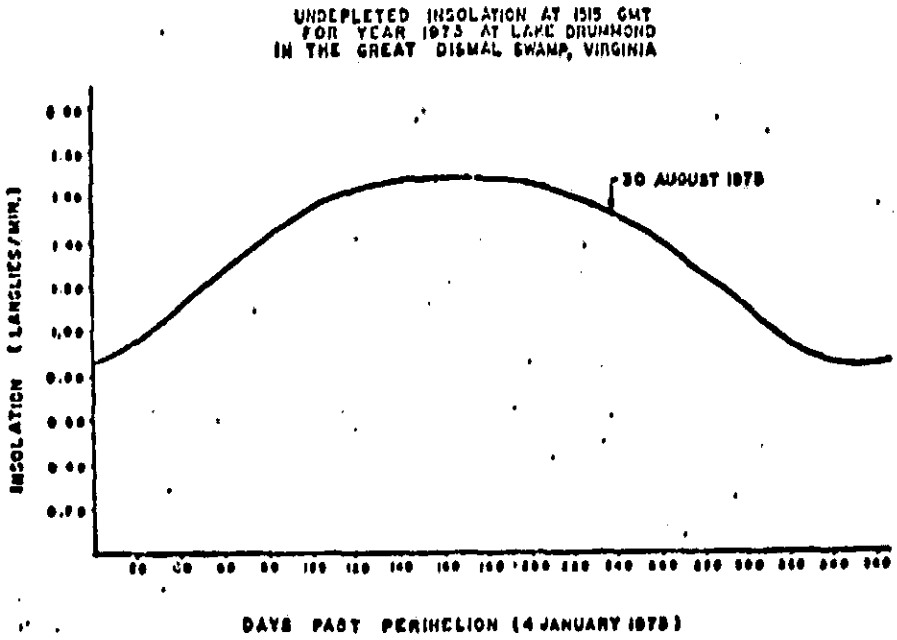

Fig. 3.

Effects of Water Vapor

Pitts, McAllum and Dillinger (1974) have discussed the effects of atmospheric water vapor on the classification accuracy of LARS when used on ERTS data. A major problem exists with MSS 7 (.8 to 1.1 microns), where water absorption bands occur. They calculated the atmospheric transmission function, including 2070 compressed water vapor lines, in a ten layer transmission model normalized to the response function of MSS 7. Using their results of average transmission versus total atmospheric water content percipitable (vertical loading), it is possible to "correct" for water vapor absorption.

ORIGINAL PAGE IS
OF POOR QUALITY

Radiosonde data from Wallops Island, Va.; Cape Hatteras, N.C.; and Washington, D.C. were used to calculate the percipitable water load for August 30, 1973. This yielded 5.8 cm in vertical and a transmission of 78%. Since the solar flux traveled a slant path (incoming) as well as a vertical path (outgoing), the total transmission for this date was 64%. No radiosonde soundings were available for October 10, 1972, but a realistic estimate for that date yields a total transmission of 75%.

If one multiplies the insolation ratio by the ratio of total transmission coefficients for those dates, then this may be used to normalize the ratios of mean radiances of training fields for those image dates. For example:

$$\frac{\mu_i}{\mu_j} = \frac{(.64)(1.244)}{.75} \qquad \text{(eq. 6)}$$

Calculations of percent difference for the quantities, yields the data shown in Table VI for water and sun angle corrected radiance ratios of 6 forest spectral classes. Positive values indicate increased reflectance.

Table VI

Water - Sun Angle Corrected Radiance Ratios

Forest spectral Class	1	2	3	4	5	6
Percent Differences	+8.2	+9.7	+6.6	+9.3	18.9	+17.6

Note that all forest classes are brighter in August. Classes 5 and 6 show the largest increase (about 19%) since these areas were logged between image dates.

CONCLUSION

Application of the LARS system in an unsupervised forest classification procedure using ERTS data has indicated that this procedure can successfully identify some plant communities in the Great Dismal Swamp. Forest spectral class means in MSS bands 4 and 5 are of little use in classification of the ground cover since those means are not sufficiently dissimilar. Classification depends almost entirely on analysis of MSS 6, 7. Seasonal changes in forest spectral statistics may be deduced from the effects of

varying sun angle, aerosol loading, and water vapor absorption, if sufficient environmental parameters are available.

Acknowledgements

We would like to thank Drs. R. N. Blais, E. C. Kindle, E. G. Astling, and Mr. T. H. Lerner who supplied technical assistance and analysis of this problem and to the personnel of Wallops Island Chesapeake Data Bank for their assistance in acquisition of aerial imagery of the Great Dismal Swamp. In addition, we would like to express appreciation to Virginia Carter, U.S.G.S., and Phil Renfroe for their assistance in this study. Financial assistance for this work was supplied through NASA grant NGL47-003-067.

References

Blais, R. N., Copeland, G. E., Lerner, T., 1975. Use of LARS System for Quantitative Determination of Smoke Plume Lateral Diffusion Coefficients from ERTS Images of Virginia, Fourth Annual Remote Sensing of Earth Resources Conference, University of Tennessee Space Institute.

Carter, V. 1974. The Dismal Swamp: Remote sensing applications. U.S. Geological Survey, National Center. 19 pp.

Erb, R. B. 1973. The Utility of ERTS-1 data for applications in agriculture and forestry. pp. 75-85. In Proc. of Third Earth Res. Tech. Satellite-1 Symposium. Vol. 1 NASA SP-351. U.S. Govt. Printing Ofc. Washington, D.C.

Heath, G. R. and H. D. Parker 1973. Forest and range mapping in the Houston area with ERTS-1. pp. 167-172. In Proc. Symp. on Significant Results obtained from ERTS-1. Vol. 1, NASA SP-327. U.S. Govt. Printing Ofc. Washington, D.C.

Heller, R. C. 1973. Analysis of ERTS imagery-problems and promises for foresters. In Proceedings Symposium IUFRO. Freiburg, Germany: 373-393.

ORIGINAL PAGE IS
OF POOR QUALITY

Lindenlaub, J. C. 1972. Remote sensing analysis: a basic preparation. LARS information note 110471. The laboratory for applications of remote sensing. Purdue University. 90 pp.

Meanley, B. 1973. The great dismal swamp. Audubon naturalist society of the central Atlantic states, Inc. 48 pp.

Pitts, D. E., McAllum, W. E., and Dillinger, A. E. 1974. The Effect of Atmospheric Water Vapor on Automatic Classification of ERTS Data. Proceedings of the 9th International Symposium on Remote Sensing of Environment, p. 483.

Potter, J. and Shelton, M. 1974. Effect of atmospheric haze and Sun Angle on Automatic Classification of ERTS-1 Data. Proceedings of the 9th International Symposium on Remote Sensing of Environment. p. 865.

Smart, W. M. 1965. Textbook on Spherical Astronomy, Cambridge Univ. Press.

Swain, Philip H. 1973. Pattern Recognition: A Basis for Remote Sensing Data Analysis. LARS Information Note 111572, Purdue Univ.

Attachment 2

USE OF LARS SYSTEM FOR THE QUANTITATIVE DETERMINATION OF SMOKE PLUME LATERAL DIFFUSION COEFFICIENTS FROM ERTS IMAGES OF VIRGINIA

USE OF LARS SYSTEM FOR THE QUANTITATIVE DETERMINATION OF SMOKE PLUME LATERAL DIFFUSION COEFFICIENTS FROM ERTS IMAGES OF VIRGINIA

R. N. Blais*, G. E. Copeland*
and T. H. Lerner†

Department of Physics and Geophysical Sciences
Old Dominion University, Norfolk, Virginia

Abstract

A technique for measuring smoke plume of large industrial sources observed by satellite using LARSYS is proposed. A gaussian plume model is described, integrated in the vertical, and inverted to yield a form for the lateral diffusion coefficient, Ky. Given $\bar{u}$, wind speed; y_1, the horizontal distance of a line of constant brightness from the plume symmetry axis a distance x_1, downstream from reference point at $x=x_2$, $y=0$, then $Ky = \bar{u}y_1^2/2x_1\ln(x_2/x_1)$. The technique is applied to a plume from a power plant at Chester, Virginia, imaged August 31, 1973 by ERTS I. The plume bends slightly to the left 4.3 km from the source and estimates yield Ky of $28 m^2 s^{-1}$ near the source, and 19 $m^2 s^{-1}$ beyond the bend. Maximum ground concentrations are estimated between 32 and 64 ugm^{-3}. Existing meteorological data would not explain such concentrations.

List of Symbols

x	= distance down wind from plume effective source
y	= horizontal distance from plume symmetry axis
z	= vertical distance from plume symmetry axis
Q	= mass per unit time of effluent emitted
$\bar{u}$	= mean scalar wind speed
$\Psi(x_1y_1z)$	= concentration of effluent as mass per unit volume

*Assistant Professor, Physics and Geophysical Sciences
†Undergraduate Technician

R. N. Blais, G. E. Copeland and T. H. Lerner

K_y	= lateral effective diffusion coefficient (l^2t^{-1})
K_z	= vertical effective diffusion coefficient (l^2t^{-1})
r	= $(x^2 + y^2 + z^2)^{\frac{1}{2}}$
$\phi(x_1y)$	= columnar loading in vertical in mass per unit area
p_{ij}	= number of i^{th} pixel in scan line j on ERTS image
λj	= number of j^{th} scan line on ERTS image
D_{ijkl}	= distance in meters from p_{ij} to p_{kl} in configuration space
α_{ijkl}	= compass bearing from ground point p_{kl} to p_{ij} in configuration space at latitude = 37^o

Introduction

Remote sensing techniques have been applied to the study of smoke plumes from fixed industrial point sources in an effort to verify numerical smoke plume dispersion models. In previous papers[1,2] the value of such studies was discussed, together with techniques that would apply to aerial photographs of plumes. In brief, such studies can aid in the development and refinement of plume dispersion models that combine stack and effluent parameters, with meteorological, or climatological data as input, and that yield ground level deposition patterns for use in air pollution control schemes and in environmental impact studies of new industrial sources. In addition, if such models exist, they can be inverted so that comparison with images of smoke plumes can yield valuable insights to regional pollution transport, wind trajectories, and vertical stability at the time the image was acquired. This is obviously useful during pollution episodes, or during field experiments.

The current study extends previous work by changing from aircraft to satellite platform (ERTS-I, recently renamed LANDSAT I) imagery, and by applying computer techniques to the analysis of the digitized imagery itself. To do this, use was made of the LARSYS software developed by the Laboratory for Applications of Remote Sensing (LARS) at Purdue University, Lafayette, Indiana, and of a remote terminal located at the National Aeronautics and Space Administration's Langley Research Center (LRC), Hampton, Virginia. The terminal gave direct access to the LARS computer and databank at Purdue, and was jointly administered by LRC and by Old Dominion University of Norfolk, Virginia.

SMOKE PLUME DIFFUSION USING LARS

For the current study a detailed analysis was made of the image of a smoke plume (ERTS E-1404-15190) as it appeared (Cf. Fg 1) about 10:00 EST, Augu s t 31, 1973. The plume arises from a steam-electric generating plant in Chester, Virginia, operated by the Virginia Electric Power Company (VEPCO), and it can be followed on the image toward the northwest about 18 kilometers. An estimate was made of the lateral diffusion coefficients as measured from the im a ge. Some anomalous meteorological conditions were examined, including an interesting large scale bend in the plume, and the fact that the wind field as reported by the nearest available meteorological stations was at odds with the observed behaviour of the plume. Finally, the plume model was run using the data acquired from the image, and estimates of ground deposition were made.

ORIGINAL PAGE IS
OF POOR QUALITY

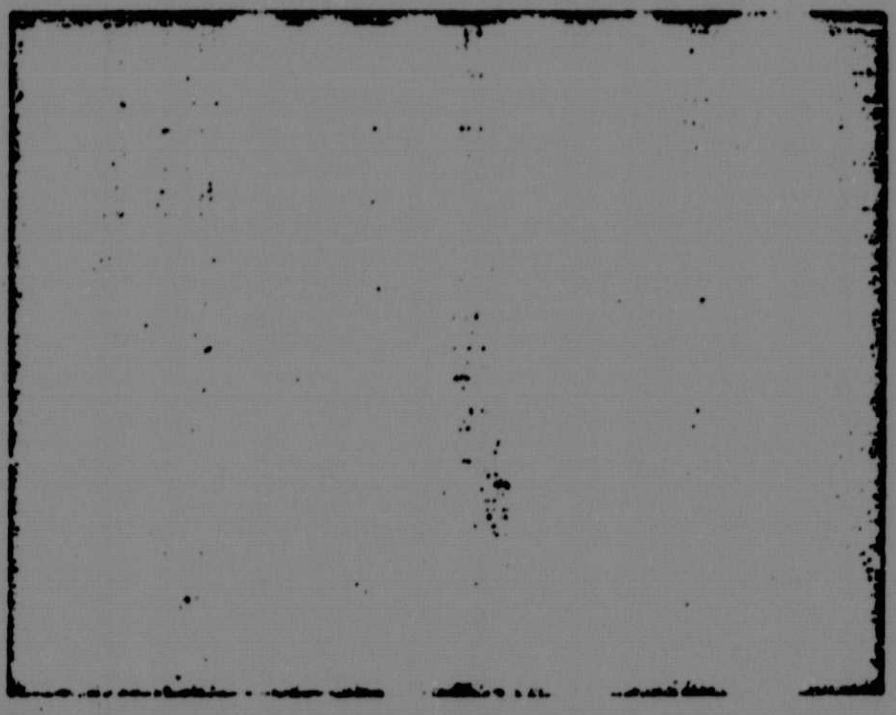

Fig. 1 Smoke plume at Chester, Virginia, 10:00 EST, as seen by ERTS MSS 4 (LARS channel 1), 31 August 1973. North is toward the top. The light vertical region branching from the plume middle is a ground feature (Army Munitions Depot).

R. N. Blais, G. E. Copeland and T. H. Lerner

Analytical Techniques

The plume model used will be briefly described outlining its required input parameters, its limiting assumptions and the forms of output it can produce. Next the type of data available through LARS will be described. Finally, two problems in relating the model to the LARS satellite data, spatial rectification of the LARS printout and computation of lateral diffusion coefficients, will be outlined.

Plume model. The computer plume model attempts to r ive a turbulent diffusion equation for a time invariant point effluent source in a wind field. The input data required is in two categories--stack and meteorological parameters. Stack parameters, available from the State Air Pollution Control Board, include stack height and diameter, and the velocity, temperature, and mass flux of the effluent. Meteorological parameters include mean wind direction and speed, surface temperature and lapse rate. Standard empirical formulas can be applied to those data to determine an "effective stack height" for the plume.[3] The plume's effective source point is usually somewhat above the true stack height due both to the vertical effluent momentum and to its buoyancy as it enters colder ambient air.

The mathematics of the turbulent diffusion equation, and its approximate solution, sometimes called the gaussian plume model, is covered in a variety of texts.[4,5] Some of its salient features will be described here. First, it assumes that the situation is steady state, both for stack and meteorological parameters. This assumption is frequently valid, but often variability in winds causes the solution to be valid only on a time average basis. Second, it is assumed that in any vertical plane normal to the mean wind vector the concentration distribution of effluent is elliptically distributed about the plume's symmetry axis with the major and minor axes aligned in horizontal and vertical directions. Third, it is assumed that the concentration falls off in any such plane along any vertical or horizontal line as a gaussian distribution centered at the major or minor axis of the ellipse. This assumption is only valid if a set of effective turbulent diffusion coefficients can be determined such that the lateral coefficient, Ky, and the vertical coefficient, K_z, are both independent of spatial and temporal coordinates and such that the downwind coefficient, K_x, is zero to first order. Boundary conditions are applied forcing concentrations to zero at large distances from the source. No effluent sinks are considered. The mass flux out the stack, Q equals $\bar{w}\bar{u}$

integrated over any plane normal to the plume's symmetry axis. Concentrations then can be described as

$$\Psi(x,y,z) = (Q/4\pi r(K_y K_z)^{\frac{1}{2}}) \exp\left((-\Omega/4x)(y^2/K_y + z^2/K_z)\right)$$

While K_z can be estimated from meteorological conditions (lapse rate, wind sheer, etc.) the determination of K_y is almost impossible from a priori considerations.

Several output forms are available from the model. One plots the concentration along any plane orthogonal to any coordinate. A second provides an output that is called the columnar loading, Φ, the definite integral of Ψ from minus infinity to plus infinity over z, which is related to brightness observed from a satellite. This is given by:

$$\Phi(x,y) \stackrel{Q}{=} (Q/(4\pi\bar{u}K_y x)^{\frac{1}{2}}) \exp\left(-\bar{u}y^2/4xK_y\right)$$

Finally, the model is capable of superimposing multiple plumes of differing stack parameters and locations, and of modifying downwind meteorological conditions.

LARS data. While the LARS system has a variety of software, only certain ones of the less sophisticated algorithms were employed. These included the LINEGRAPH, COLUMNGRAPH, and PICTUREPRINT programs. The LINEGRAPH program will take any scan line of any spectral band, and will prepare a graph of the radiance as a function of pixel (picture element) number along the scan line. The COLUMNGRAPH feature plots radiance versus scan line number for a given pixal number. Finally, PICTUREPRINT prepares a greyscale map of a region in a single ERTS spectral band with an option to assign up to 16 symbols to 16 different grey scale domains specified by the user. When used in conjunction with auxiliary programs (HISTOGRAM and GRAPHISTOGRAM) it is possible to density slice the map in such a way that background is completely suppressed (i.e. printed as a blank), while a feature of interest (e.g. a smoke plume) is printed in several symbols representing differing regions of brightness or reflectivity. Figure 1 shows such a printout though photoreduction for publication has made it hard to distinguish the different symbols. Lines of constant brightness can then be projected on the horizontal plane, and the first two graphing programs can be used to determine inflection points on the spatial brightness curve, yielding lines of maximum contrast that can be superimposed by hand on the grey scale map.

Fig. 2 LARSYS PICTUREPRINT of smoke plume. ERTS MSS 4 (LARS 1)

LARSYS PICTUREPRINT Spatial Rectification. The grey scale maps printed by the LARS System (LARSYS) are spatially distorted. ERTS is in a near polar orbit at 99° to equator. Thus, the ground truck is not along lines of constant longitude. The MSS scans perpendicularly to the ground track of the satellite. Thus the MSS image is a parallogram projected on the earth's surface. In any given line a pixel of a certain number represents a point slightly west of the point due south of the similarly numbered pixel in the preceding line. The computer's printer inherently prints pixels of identical number directly beneath one another. Moreover, the number of typed symbols per line, and lines per inch do not correspond directly to the actual ground scene spacing of areas represented by pixels and lines. To correct these problems, three simple formulas were developed so that true distances and compass bearings could be determined from a LARSYS PICTUREPRINT. Select two pixels Pij and Pkl on scan lines j and l, then the actual distance in meters, D_{ijkl}, between the two points on the ground is given by

$$D_{ijkl} = (79m)((\lambda_l-\lambda_j)^2 + (p_{ij}-p_{kl})^2(0.494))^{\frac{1}{2}}$$

ORIGINAL PAGE IS
OF POOR QUALITY

SMOKE PLUME DIFFUSION USING LARS

The azimuthal angle, α_{ijkl}, in degrees measured to the east of north between the two pixels is then

$$\alpha_{ijkl} = 10^{o} + \tan^{-1}((p_{ij}-p_{kl})(0.70)/(\lambda_1-\lambda_j))$$

Finally, we will be interested in measuring horizontal plume widths on grey scale maps along lines perpendicular to the downwind symmetry axis of the plume. Thus, given two pixels, p_{ij} and p_{kl}, on that symmetry axis, we would like to find another pixel, p_{mn}, in any line, l_n of our choosing that represents a point on a line passing through p_{ij} perpendicular in configuration space to the plume axis. This is given by

$$p_{mn} = p_{ij} + (2.02)((\lambda_n-\lambda_j)(\lambda_1-\lambda_j)/(p_{ij}-p_{kl}))$$

Theory for determination of the lateral diffusion coefficient. In a previous publication[2] measurements of lateral diffusion coefficient by eye from aerial photos were reported. The eye detects the "shape" of the plume as the line of maximum contrast between plume and background, and not as a line of constant brightness. In that case it was reported that the shape of the line of maximum concentration is parabolic, with the apex at the source, and in accordance with the model it satisfies the formula:

$$y = (2K_y x/\bar{u})^{\frac{1}{2}}$$

Through the LARSYS PICTUREPRINT program it is possible to determine lines of constant brightness. We may assume these are related to lines of constant columnar loading, as long as the plume is not opaque, and is of sufficiently low concentration for multiple light scattering events to be insignificant. The shape of such a line can be derived from Eq2 by setting $\Phi(x_2,0)=\Phi(x_1,y_1)$. The result is

$$\tfrac{1}{2}Q(\pi\bar{u}K_y x_2)^{-\frac{1}{2}} \simeq \tfrac{1}{2}Q(\pi\bar{u}K_y x_1)^{-\frac{1}{2}}\exp(-\bar{u}y_1^2/4x_1K_y)$$

This can be solved for the contour of lines of constant brightness.

$$y_1 = ((2x_1K_y/\bar{u})\ \ln\ (x_2/x_1))^{\frac{1}{2}}$$

Such lines form closed contours (Cf Fg. 3) and if x's and y's can be determined experimentally from measurements on a gray scale map one can solve for Ky

$$K_y \simeq \bar{u}y_1^2/(2x_1\ \ln\ (x_2/x_1))$$

Thus, in theory, the lateral diffusion coefficient can be measured.

Practical considerations. Due to the fact that a real, turbulent plume is being interpreted with the aid of an idealized time averaged model, it is insufficient to use one set of data points (x's and y's) to determine the lateral diffusion coefficient. A graphic overlay technique is used to smooth data so that a series of data points are used to determine an average value of Ky. In essence, a plume symmetry axis is drawn on the gray scale map by eye. Second, a series of lines perpendicular to it are marked out using the spatial rectification procedure. Then a smooth outline of the plume's lines of constant brightness are sketched. Widths are measured as a function of downwind distance, Ky's are computed and averaged. These are then used as input to the plume model.

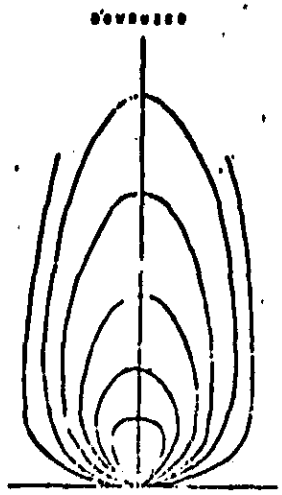

Fg 3. Lines of constant brightness as seen from above.

One other point is that different ERTS spectral bands give different results. This is to be expected since the ability of smoke particles to scatter light is strongly dependent on particle size and optical wave length. ERTS band 7 (LARS band 4) in the near infra-red (0.8 - 1.1um) cuts through haze readily, and frequently a plume that is very visible in another band is almost undetected in band 7. This may prove to be a useful tool for obtaining a crude size distribution for plume aerosols.

Analysis of the Chester, Virginia, Plume

A beautiful example of an industrial smoke plume was imaged by ERTS-1 on Friday, August 31, 1973, arising from an oil fired power generating station at Chester, Virginia. All input information needed to run the model could be obtained, and the image was taken with ideal atmospheric conditions. Thus, it was decided to analyze the case in detail. The source of the plume will be described, as will the meteorological conditions. A peculiar bend in the plume will be briefly discussed, then lateral diffusion coefficients will be estimated. Finally, the results of

the plume model run using those values of Ky will be discussed.

Plume source. The power plant at Chester, Virginia is located on the south bank of the James River, 17 km NNE of Petersburg, and 19 km SSE of Richmond. The plant has six smoke stacks. The height, h; internal diameter, I.D.; effluent efflux velocity, v; effluent temperature, T; and rate of fuel (No. 6 oil) consumption, f, are tabulated below.

Stack	h(m)	I.D.(m)	$v(ms^{-1})$	T(°C)	$f(kgs^{-1})$
1	61	3.7	12	197	5.91
2	61	3.7	15	174	7.96
3	61	4.0	14	142	9.75
4	61	4.0	22	162	15.0
5	61	5.2	23	130	29.3
6	61	6.1	33	128	58.9

Meteorological conditions. The analysis of meteorological conditions at the time the plume was imaged presents a conundrum, because the reports of the nearest stations indicate a situation at odds with the observed plume behavior. Eastern Virginia was under the influence of a weak high pressure system with associated light breezes. Winds reported at Richmond were calm at 9:58 EST and reached 7 knots from 200° (SSW) at 10:56 EST. The satellite imaged the scene at 10:14 EST (15:14 Z). From sunrise until 9:58 EST, the temperature had risen rapidly from 69°F to 89°F at a rate of about 5°F/hour, but from 9:58 EST until 10:56 EST the temperature rose only 2°F, and during the following hour it failed to rise at all. Such behavior would indicate that a weak diurnal inversion persisted over the region until the morning insolation caused sufficient heating of the earth's surface to warm the lower layer of air. When the inversion broke up, sometime between 9:58 EST and 10:56 EST a much thicker mass of air had to be heated resulting in the decreased rate of temperature increase. Though no radiosondes are flown from Richmond, the nearest ones (from Wallops Island, Virginia, and from Washington, D. C.) do indicate the presence of such an inversion that morning.

The presence of this inversion, and its breaking up, is in accord with the observed plume behavior, but the wind directions are not. All surrounding stations reported winds out of generally southwesterly directions, yet the plume

clearly was heading off toward the northwest, thus being blown by southeasterly winds. The significance of this fact will be discussed in the conclusions, while the accord with the inversion will be discussed in the next section.

Bend in Plume. An obvious feature of the plume is that it bends. Starting from the source, the plume heads 4.3 km at an azimuth of 305°, then turns westward at 272°. At first this bend was assumed to indicate the rise of the plume to a higher altitude with differing flow direction, but this peculiar bend to the left was not consistent with the tendency of winds at higher altitudes to blow at an angle to the right of the surface winds. The idea was proposed to the authors by Herman Wobus and Earl Kindle that the bend did not represent a spatial variation in the windfield, but rather a temporal one. Prior to approximately one half hour before the image was acquired, the wind did blow from the east carrying the plume away from the source at 272°. Then it shifted to a more southeasterly wind that carried the effluent subsequently discharged off in a bearing of 305°. This wind shift is associated with downward momentum transfer after the breaking up of the inversion. But significantly, the new wind direction carried the older plume, still with its symmetry axis oriented at 272° bodily off at 305°. This changed the Ky value obtained for portions of the plume farther from the source than 4.3 km from the value obtained closer to the source. Thus, two different lateral diffusion coefficients were to be expected for the two regimes. Wobus predicted, in fact, that a smaller Ky in the more distant portion of the plume could allow higher concentrations to occur at the bend point (a virtual source) than would be experienced closer to the real stack. Superficially, an examination of the greyscale maps indicated a region of enhanced brightness was indeed present, but it has so far been impossible to definitively establish that it is not related to a ground feature, a large military depot, that is unfortunately right beneath the bend. A LARSYS CLASSIFYPOINTS program did remove the background feature leaving the bright downstream region, but its photometric interpretation is difficult. When the two values of Ky determined from the imagery were inserted in the plume model, it did display the feature Wobus predicted.

Determination of Lateral Diffusion Coefficients. The coefficients determined by the method above can be determined as a function of wind speed. Between the source and the bend care had to be exercised to not allow the multiple stacks to confuse the issue by causing an apparent

broadening of the plume that would be interpreted as an excessively large value of Ky. Thus, only a limited number of points of adequate downstream distance could be used. The mean value was determined to be Ky=11.6 (m) $\bar{u} \pm 0.6$ (m) $\bar{u}$. In the region beyond the bend more numerous measurements lead to values of Ky = 8.0 (m)$\bar{u} \pm$ 1.6 (m)$\bar{u}$.

Wind speeds were now estimated by noting that the bend in the plume is 4.3km from the source. The meteorological data indicated the inversion was breaking up around the time of the last observation at 9:58 EST. Assuming the wind shifted about a half hour before the satellite pass, the wind speed would have to be approximately 8.6km per hour, or to one significant figure 6 knots. This makes the values of diffusion coefficient between source and bend Ky = 28 $m^2 s^{-1}$. This value is probably overestimated due to apparent broadening of multiple sources. Assuming a similar windspeed beyond the bend, the value would bw Ky = 19 $m^2 s^{-1}$. Both these values are of course based on crude assumptions.

Model predicted ground concentrations. Inserting the above values into the plume model, together with stack and meteorological parameters, the following output (Fg 4) was produced. Concentrations at ground level are printed on a binary exponential scale, such that a 2 indicates 2^2 ugm^{-3}, and a 5 would indicate 2^5 ugm^{-3}, etc.

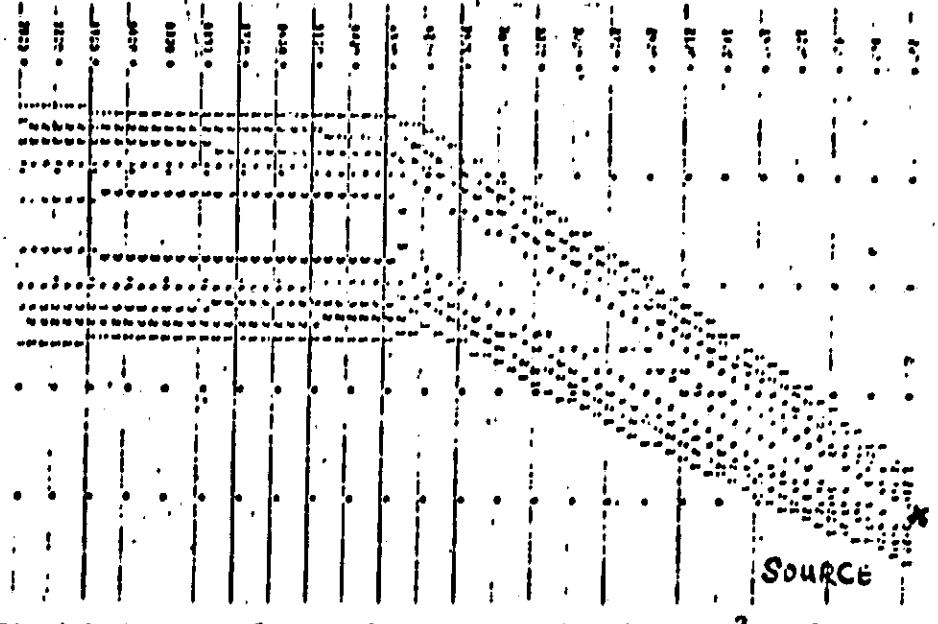

Fig 4 Printout of ground concentration in ugm^{-3} on binary exponential scale. Vertical lines measure distance downstream from the source in 100m units.

ORIGINAL PAGE IS
OF POOR QUALITY

Maximum ground concentration inside the region marked 5 would be greater than 2^5 or 32 ugm^{-3}, but less than 2^6 or 64 ugm^{-3}.

Conclusions

The application of satellite imagry to the analysis of smoke plumes has shown that useful data can be acquired that could not be assembled in any other way. First, anomalously high particulate pollution levels that would potentially be recorded by surface air quality stations would have been attributed to the wrong cause on the test day simply because the nearest meteorological stations reported different wind directions. Consequently, local air pollution models for urban regions that depend on a limited number of reporting stations should be checked against remotely sensed data to identify the extent and and frequency of such anomalous behavior. Second, the smoke plume itself records a temporal history of the day's meteorological conditions, filling in gaps in locally recorded data. Finally, if emission parameters are known satellite data can lead to reasonable estimates of surface loading due to a plume simply by seeing its apparent geometric shape.

Acknowledgements

We would like to thank numerous people for providing assistance to this study: first, Dr. E. C. Kindle of ODU, who stimulated the project, secured funds for its completion and suggested many of the central ideas; Mr. H. Wobus of ODU, who elegantly programmed the model and suggested the reason for the bend in the plume; Mr. John Salop of the Virginia Air Pollution Control Board who secured the emission data; finally to NASA grant NGL47-003-067, funded through Wallops Island Station that provided financial.support.

References

[1]Blais, R. N., "Inherent Limitations of Monocular Techniques for Determining Smoke Plume Parameters from Aerial Photography: An Error Analysis," Remote Sensing of Earth Resources, Vol. 3, University of Tennessee Space Institute, Tullahoma, Tenn., 1974.

[2]Hilton, G. M. and R. N. Blais, "Determination of Physical Parameters of Smoke Plumes from Aerial Photographs for Input to Computer Plume Models," ibid.

[3]Committee on Air Pollution Controls, Recommended Guide for the Prediction of the Dispersion of Airborne Effluents, (New York, N. Y.: The American Society of Mechanical Engineers, 1968), pp. 36-40.

[4]Sutton, O. G., Micrometeorology (New York: McGraw-Hill, Inc, 1953) pp. 135-140, 292-295.

[5]Copeland, G. E., et al, Correlation of Satellite and Ground Truth Data in Air Pollution Studies (unpublished technical proposal to NASA, Old Dominion University Research Foundation, 20 January 1973), pp. I-17 - I-33.

ORIGINAL PAGE IS
OF POOR QUALITY